

Article

Mo₂C-Based Microfluidic Gas Sensor Detects SF₆ Decomposition Components: A First-Principles Study

Li Liu ¹, Guozhi Zhang ^{1,2,*}, Zengting Wang ¹, Jiawei Yuan ¹ , Senyuan Tan ¹ and Yi Li ³¹ School of Electrical and Electronic Engineering, Hubei University of Technology, Wuhan 430068, China² Hubei Engineering Research Center for Safety Monitoring of New Energy and Power Grid Equipment, Hubei University of Technology, Wuhan 430068, China³ School of Electrical Engineering and Automation, Wuhan University, Wuhan 430072, China

* Correspondence: zhangguozhi@hbut.edu.cn

Abstract: Mo₂C is a two-dimensional material with high electrical conductivity, low power consumption, and catalytic effect, which has promising applications in the field of microfluidic gas detection. First principles were used to study the adsorption characteristics of Mo₂C monolayer on four typical decomposition gases of SF₆ (H₂S, SO₂, SOF₂, and SO₂F₂), and to explore the feasibility of its application in the detection of SF₆ decomposition components. The results showed that Mo₂C chemisorbed all four gases, and the adsorption capacity was H₂S < SO₂ < SOF₂ < SO₂F₂. The adsorption mechanism of Mo₂C as a microfluidic sensor was analyzed in combination with its charge-density difference and density of states. On the other hand, the different work-function change trends after adsorbing gases provide the possibility for Mo₂C to selectively detect gases as a low-power field-effect transistor sensor. All content can be used as theoretical guidance in the realization of Mo₂C as a gas-sensitive material for the detection of SF₆ decomposition components.

Keywords: Mo₂C; gas detection; first principles; SF₆ decomposition components

Citation: Liu, L.; Zhang, G.; Wang, Z.; Yuan, J.; Tan, S.; Li, Y. Mo₂C-Based Microfluidic Gas Sensor Detects SF₆ Decomposition Components: A First-Principles Study. *Chemosensors* **2022**, *10*, 368. <https://doi.org/10.3390/chemosensors10090368>

Academic Editor: Eleonora Alfinito

Received: 11 August 2022

Accepted: 14 September 2022

Published: 16 September 2022

Publisher's Note: MDPI stays neutral with regard to jurisdictional claims in published maps and institutional affiliations.



Copyright: © 2022 by the authors. Licensee MDPI, Basel, Switzerland. This article is an open access article distributed under the terms and conditions of the Creative Commons Attribution (CC BY) license (<https://creativecommons.org/licenses/by/4.0/>).

1. Introduction

SF₆, as a gas medium with excellent insulation and arc extinguishing properties, plays an important role in reducing the footprint of high-voltage equipment and optimizing the installation design, etc. [1–3]. Because of the excellent chemical properties of SF₆ insulating gas, it is more and more widely used in the field of electric power. During its long-term operation, SF₆ will be decomposed due to partial discharge and partial overheating, and the generated series of products will react with the moisture and oxygen present in the equipment to produce a stable mixture of gas components, represented by H₂S, SO₂, SOF₂, and SO₂F₂ [4,5]. The presence of these gases will reduce the insulation performance of SF₆, and eventually lead to equipment failure. Studies have shown that the type and content of these gases can be used to determine the type, size, and cause of partial discharges and to provide reliable information for assessing the insulation status of the equipment [6,7]. Therefore, it is necessary to test these gases to ensure the insulation status of electrical equipment.

A microfluidic gas-sensing-and-detection method based on nano gas-sensitive materials has received wide attention for its high sensitivity, high selectivity, high reliability and long-term stability, and it is the future development direction of built-in sensing and online monitoring of gas insulation equipment due to its high integration and small size. With nanogas-sensitive materials as its core working part, many scholars have done a lot of research work from theory to experiment on the gas-sensitive properties of these materials: transition metal sulfides represented by MoS₂ [8,9], transition metal carbides represented by GaN, InN [10–12], metal oxides represented by SnO₂, ZnO [13,14], etc. More and more gas-sensitive materials are being developed and utilized. Mo₂C, as one of the transition metal carbide nanomaterials, has been used in various application studies because of its

superior physical, chemical, and mechanical properties. Soo-Yeon Cho et al. [15] used molybdenum carbide to fabricate solid-state gas sensors with high sensitivity and stability. Wang Tao et al. [16] theoretically investigated the relationship between the stability of different Mo₂C surfaces and CO adsorption. In particular, Mo₂C has a high conductivity similar to that of pure metals [17], which offers the possibility to be used as low-power device development.

Two-dimensional Mo₂C planes were selected as gas adsorption surfaces for the study, and firstly, various adsorption structures of four typical SF₆ decomposition components, SO₂, SOF₂, SO₂F₂, and H₂S, were constructed on the Mo₂C surface, respectively. The optimal adsorption configuration of each adsorption system is derived from the adsorption energy, and then the chemical interaction between the gas molecule and the surface and the electronic structure of the system are investigated for each adsorption structure, and the Charge Density Difference (CDD) and Density of States (DOS) are calculated to analyze the bonding between the atoms and the surface within the adsorbed molecule in detail. In order to further explore and broaden the possibility of the application of Mo₂C-based microfluidic devices in practical engineering, the theoretical desorption time of each adsorption system and the possibility of application in field-effect transistor sensors were calculated in this paper. The interaction behavior of the Mo₂C surface and SF₆ decomposition components is discussed in depth in theoretical calculations, which provides a theoretical basis for developing Mo₂C-based microfluidic gas sensors with better adsorption performance for SF₆ decomposition component detection [18–21].

2. Computational Details and Models

All models were constructed under the Materials Studio software and all calculations were performed under the Dmol³ module [22]. The Perdew–Burke–Ernzerhof (PBE) generalized function of the Generalized Gradient Approximation (GGA) method was adopted to handle the exchange correlations of the electron parts [23]. The p-polarized double numerical polarization (DNP) is adopted as the basis set function of the atomic orbital. Since Mo is a transition metal element, the dispersion-corrected density functional theory (DFT-D) method developed by Tkachenko and Scheffler and the TS method are used to understand the weak interaction and van der Waals force, instead of using Grimme’s empirical diffusion-corrected DFT-D [24]. The orbital truncation radius was set to 5.0 Å (1 Å = 1 × 10^{−10} m) [25]. For the geometry-optimized relaxation of all structures, the convergence criteria were set as follows: the difference in energy between the two geometry optimizations was less than 1.0 × 10^{−5} Ha (1 Ha = 27.21 eV), the force per atom was less than 0.002 Ha/Å, and the maximum displacement distance per atom was less than 0.005 Å [26]. For the electron step iteration in each geometry optimization step, the energy difference between the two calculations is less than 1.0 × 10^{−6} Ha.

A 4 × 4 × 1 monolayer of Mo₂C contains 16 C atoms and 32 Mo atoms, and a 15 Å vacuum layer is set up to eliminate the effect of interlayer interactions.

The four gas molecules approach the Mo₂C surface in different orientations to finally obtain multiple adsorption structures with minimum total local energy. Among them, the adsorption energy (E_{ads}) of a single gas molecule on the Mo₂C surface is calculated as [27]:

$$E_{ads} = E_{monolayer + gas} - E_{monolayer} - E_{gas} \quad (1)$$

where $E_{monolayer + gas}$ is the total energy of the system after adsorption of gas molecules on the Mo₂C surface, $E_{monolayer}$ is the energy of Mo₂C, and E_{gas} is the energy of gas molecules; if E_{ads} is negative, it indicates that this is a spontaneous and stable exothermic reaction [28].

Mulliken’s method was used to analyze the charge transfer between the gas molecules and the adsorbed substrate, and the corresponding calculation equation is shown below:

$$\Delta Q = Q_1 - Q_2 \quad (2)$$

where Q_1 represents the charge of the gas molecule after adsorption, and Q_2 represents the charge of the gas molecule before adsorption, and define ΔQ to quantify the charge change; if ΔQ is positive, it indicates that the gas molecule loses electrons and the crystal surface gains electrons during the adsorption process, and the opposite if ΔQ is negative [29].

3. Results and Discussion

A model of the most stable two-dimensional Mo_2C is shown in Figure 1a. The structure is derived from the 111 surface of the cubic Mo_2C with the original lattice parameter of $a = 4.155 \text{ \AA}$. Mo_2C is a typical three-layer interlayer material with a top view demonstrating a graphene-like six-membered ring structure, a configuration similar to other reported two-dimensional transition metal sulfides typified by MoS_2 [30]. The band structure of two-dimensional Mo_2C is shown in Figure 1b, and the calculated results show a band gap of 0, confirming its high conductivity with a metallic nature [17]. Figure 1c shows the structures of the four gas molecules, from which it can be seen that the structures of the four gas molecules are basically symmetrical. Combining the setting scheme of the adsorption sites and the structural characteristics of the gas molecules in the relevant adsorption studies, three different adsorption configurations were constructed for H_2S , SO_2 gas molecules, while four different adsorption configurations were constructed for SOF_2 and SO_2F_2 gases. The data such as adsorption energy for the best adsorption configuration of the four gas molecules are shown in Table 1. The adsorption energy of MoS_2 (Pt-doped) [31] for SO_2F_2 , SOF_2 is -1.39 eV and -2.65 eV , respectively, while the adsorption energy of GaN (Cr-doped) [4] for H_2S and SO_2 is -1.02 eV and -2.84 eV , respectively, which is significantly larger than that of Mo_2C . In order to better analyze the adsorption behavior of Mo_2C on these four gases, the HOMO (Highest Occupied Molecular Orbital)-LUMO (Lowest Unoccupied Molecular Orbital) energies of these four gases were calculated, and the specific values are shown in Table 2. SO_2F_2 has the largest energy gap, followed by SOF_2 , SO_2 and H_2S , which indicates that the SO_2F_2 molecule is the most stable. In terms of HOMO energies, SO_2F_2 is the largest, which means that it is the least bound, so it is the most active and the most variable, which is verified by the adsorption energy. In the next section, the adsorption behavior of the four gas molecules will be discussed in depth in terms of the band structure, DOS, and charge transfer.

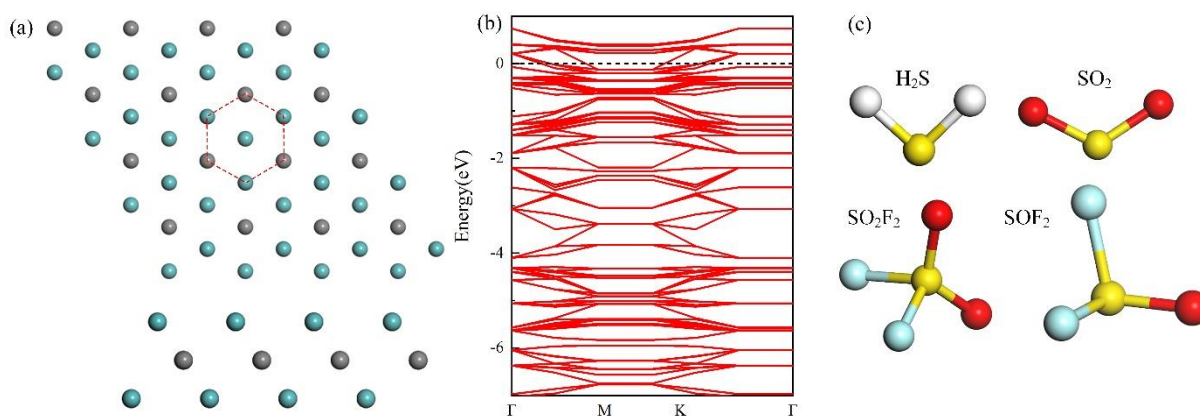


Figure 1. (a) most stable conformation, (b) band structure of Mo_2C and (c) four molecular models.

Table 1. Adsorption energy (E_{ad}), adsorption distance (D), and transferred charge (Q) for the best adsorption configuration of four gas molecules on Mo_2C . D (Å) is the distance between the gas molecule and the nearest atom of the adsorption substrate; Q (e) is the charge transfer between the gas molecule and the adsorption substrate.

Molecule	E_{ad} (eV)	D (Å)	Q (e)
H ₂ S	−1.560	2.543	0.125
SO ₂	−2.538	2.152	−0.224
SOF ₂	−3.458	1.888	−0.643
SO ₂ F ₂	−4.944	1.511	−0.488

Table 2. HOMO/LUMO energies of the four gas molecules.

Molecule	HOMO (eV)	LUMO (eV)	Energy Gap
H ₂ S	−0.226	−0.069	0.157
SO ₂	−0.301	−0.180	0.121
SOF ₂	−0.319	−0.121	0.198
SO ₂ F ₂	−0.342	−0.108	0.234

3.1. Adsorption Characteristic of Mo_2C

Based on the obtained most stable Mo_2C configuration, for the H₂S adsorption system, three different adsorption models: H₂S molecules parallel to the Mo_2C surface, two H atoms facing downward perpendicular to the Mo_2C surface, and S atoms facing downward perpendicular to the Mo_2C surface were constructed respectively to perform adsorption calculations, and the most stable configuration of H₂S gas molecules adsorbed on the Mo_2C surface was obtained according to the adsorption energy calculation formula (Equation (1)), as shown in Figure 2a. It is obvious from the figure that H₂S interacts with Mo_2C in a form slightly parallel to the Mo_2C surface as a whole, with an adsorption energy of −1.560 eV, which is less than −0.800 eV, and it is easy to conclude that the adsorption of H₂S is chemisorption [32]. Further analysis shows that the adsorption distance of H₂S is 2.543 Å and there is no significant deformation of the H₂S molecular structure after adsorption, and from the Mulliken aspect, Mo_2C gets 0.125 e after the adsorption is completed. As seen in the corresponding CDD of Figure 3c, there is a more obvious overlap of electron dissipation and accumulation between the downward-facing F atom and the two O atoms and the Mo atom below it, explaining the interaction between them [33]. Similar to the H₂S adsorption system, three different adsorption models: SO₂ molecules parallel to the Mo_2C surface, two O atoms facing downward perpendicular to the Mo_2C surface, and S atoms facing downward perpendicular to the Mo_2C surface were constructed to perform adsorption calculations. The most stable configuration of SO₂ gas molecules adsorbed on the Mo_2C surface was obtained, as shown in Figure 2b. It is obvious from the figure that SO₂ is adsorbed on the Mo_2C surface in the form of two O atoms facing downward and S atoms facing upward, with an adsorption energy of −2.538 eV, it is easier to conclude that the adsorption of SO₂ is chemisorption. Upon further analysis, the adsorption distance of SO₂ is 2.152 Å, and there is no significant deformation of the SO₂ molecular structure after adsorption, and from the Mulliken aspect, Mo_2C loses 0.224 e after the adsorption is completed. The electron transfer process of SO₂ adsorption on the Mo_2C surface can be directly seen in the corresponding CDD of Figure 3b. A large amount of blue charge accumulation is wrapped around the whole SO₂ molecule, while the Mo atom directly below is surrounded by a yellow charge dissipation region, verifying the electron gaining behavior of SO₂ during the adsorption. The interaction between the O atom and the Mo atom below it is explained by the presence of a certain overlap of electron dissipation and accumulation.

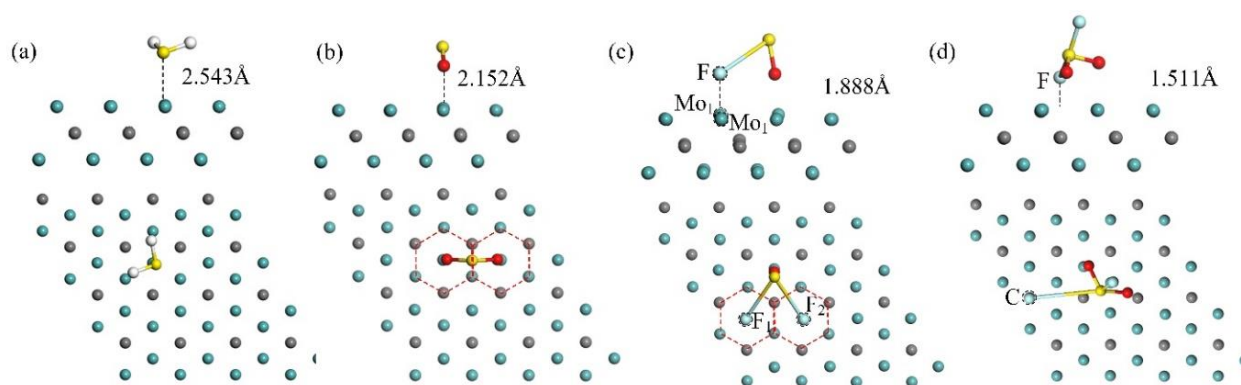


Figure 2. Most stable conformation of H₂S (a), SO₂ (b), SOF₂ (c) and SO₂F₂ (d) systems.

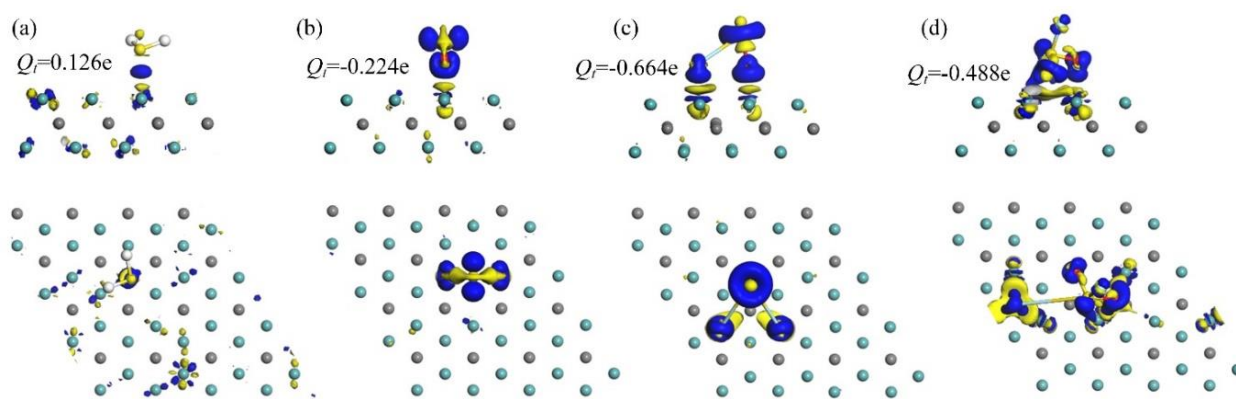


Figure 3. CDD of H₂S (a), SO₂ (b), SOF₂ (c) and SO₂F₂ (d) systems. In CDD, the blue area is electron accumulation and the yellow area is electron depletion, with an isosurface of 0.05 e/Å³.

For the SOF₂ adsorption system, four different adsorption models were constructed with S atoms facing the Mo₂C surface and other atoms facing up, S atoms facing up and other atoms facing the Mo₂C surface, O atoms facing the Mo₂C surface and other atoms facing up and F atoms facing the Mo₂C surface and other atoms facing up, respectively. The most stable configuration of SOF₂ gas molecules adsorbed on the Mo₂C surface was obtained, as shown in Figure 2c. It is obvious from the figure that SOF₂ is adsorbed on the Mo₂C surface in the form of two F atoms and one O atom facing downward and sulfur atoms facing upward, with an adsorption energy of -3.458 eV, which is a more obvious chemisorption. Further analysis shows that the adsorption distance of SOF₂ is 1.888 Å. After adsorption, the two F atoms of the SOF₂ molecule are obviously far away from the molecular body and finally located directly above the Mo atom, respectively. Mo₂C loses 0.634 e after the adsorption is completed. As seen in the corresponding CDD of Figure 3c, there is a more pronounced overlap of electron dissipation and accumulation between the downward-facing O atom and the two F atoms and the Mo atom below them, explaining the stronger interaction between them. For the SO₂F₂ adsorption system, four different adsorption models were constructed with S atoms facing the Mo₂C surface and other atoms facing upward, F atoms facing the Mo₂C surface and other atoms facing upward, two O atoms facing the Mo₂C surface and other atoms facing upward and two F atoms facing the Mo₂C surface and other atoms facing upward. The most stable configuration of SO₂F₂ gas molecules adsorbed on the Mo₂C surface was obtained as shown in Figure 2d. It is obvious from the figure that SO₂F₂ is adsorbed on the Mo₂C surface in the form of one F-atom facing upward, two O atoms facing slightly downward, and another F atom facing downward, with an adsorption energy of -4.944 eV, which is a more obvious chemisorption as well. Further analysis shows that the adsorption distance of SO₂F₂ is 1.511 Å. After adsorption, one F atom of the SO₂F₂ molecule is far away from the molecular body and

finally located directly above the C atom. From the Mulliken aspect, Mo_2C loses 0.488 e after the adsorption is completed. From the corresponding CDD in Figure 3d, it can be intuitively seen that the electron dissipation and accumulation with large overlap between SO_2F_2 and its underlying Mo atoms explain the strong interaction between them.

3.2. Electronic Behavior

The band structure of the most stable adsorption configuration of H_2S is shown in Figure 4a. Compared with the band structure of the Mo_2C substrate before adsorption, the band gap value remains zero, but the band near the Fermi level increases. To further analyze the adsorption mechanism, the DOS is plotted as shown in Figure 5(a1,a2). There is no change in the total DOS at the Fermi level after the adsorption of H_2S by Mo_2C , while the partial overlap of the S 3p orbitals and their nearest Mo 4d orbitals can be seen from the partial density of states map, but the overlap region is small due to the small percentage of the Mo 4d orbital region. This means that there is a certain orbital hybridization between H_2S and Mo_2C , which means that there is some interaction between them [34]. The band structure of the most stable adsorption configuration of SO_2 is shown in Figure 4c, compared with the band structure of the Mo_2C substrate before adsorption, the band gap value remains 0 without change, but the energy band near the Fermi level increases further compared to the H_2S adsorption system. The DOS is plotted for further analysis of the adsorption mechanism, as shown in Figure 5(b1,b2), the trend of the total density of states changes is unchanged after the adsorption of SO_2 by Mo_2C , but the peak at -0.4 eV increases compared to that before the adsorption, and the change of this peak is known from the corresponding partial density of states plots contributed by the Mo 4d orbital. Similarly, the peak around -4.4 eV is contributed by the O 2p orbital. In terms of the degree of the partial density of states crossover, the O 2p orbitals and Mo 4p orbitals are more crossed at -3 eV to -5 eV and less crossed at -2 eV– 1 eV. Overall, the orbital hybridization existing between SO_2 and Mo_2C is stronger than that of the H_2S adsorption system, which is also verified in the adsorption energy.

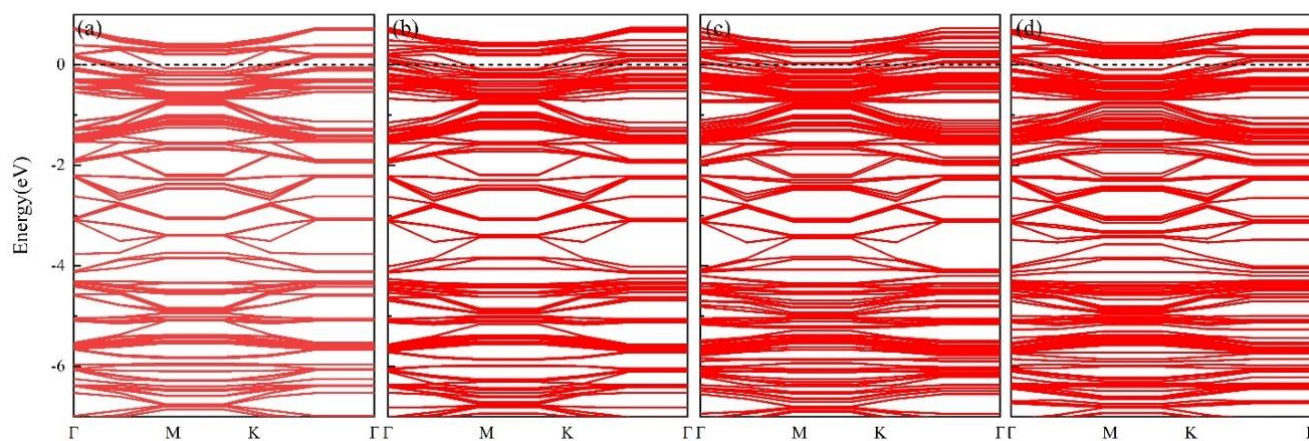


Figure 4. Band structures of H_2S (a), SO_2 (b), SOF_2 (c) and SO_2F_2 (d) systems. The dash line is the Fermi level.

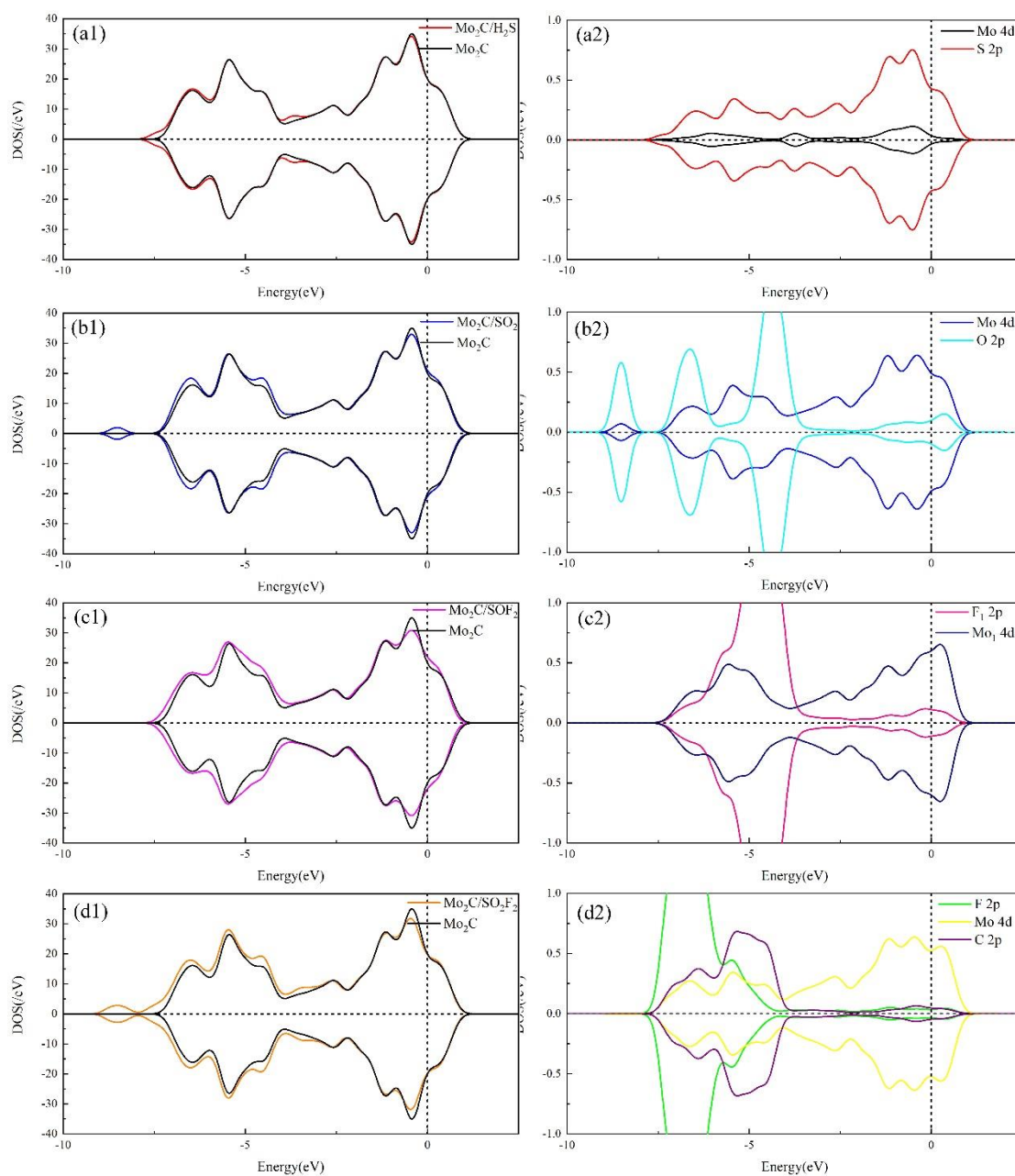


Figure 5. DOS of H₂S (a1,a2), SO₂ (b1,b2), SOF₂ (c1,c2) and SO₂F₂ (d1,d2) systems. The dash line is the Fermi level.

The band structure of the most stable adsorption configuration of SOF₂ is shown in Figure 4c, and its band gap value is the same as that of the Mo₂C substrate before adsorption, but the energy band near the Fermi level is further increased compared with that of the SO₂ adsorption system. The peak at -0.4 eV is lower than that before adsorption, but the DOS in the region to the left of -3.5 eV is higher than that before adsorption. Overall, the orbital hybridization existing between SOF₂ and Mo₂C is stronger than that of the SO₂ adsorption system. Figure 4d shows the band structure of the most stable adsorption configuration of SO₂F₂, where the band gap value is the same as that of the Mo₂C substrate before adsorption, but the energy band near the Fermi level is further increased compared to the other three adsorption systems. The corresponding partial density of states plots shows that the F 2p orbitals, Mo 4d orbitals, and C 2p orbitals in the corresponding range have different degrees of crossover, and the degree of crossover at the Fermi level is relatively small. In general, the orbital hybridization between SO₂F₂

and Mo₂C is the strongest among the four adsorption systems, which is also verified in the adsorption energy.

Through the analysis of the above four adsorption systems, it was found that Mo₂C is in contact with the four SF₆ decomposition component gas, the adsorption energy is larger, more easily captured by the Mo₂C surface, and its surface electron transfer, resulting in an increasing in the energy band, but the band structure shows that it still shows metallic, which increases the possibility of Mo₂C as low-power gas-sensitive sensing materials for industrial applications. The next section will explore other applications in terms of low-power material properties. The feasibility of industrial applications of Mo₂C will be further explored in the next section in terms of the theoretical sensing response and recovery time of gas-sensitive sensors.

3.3. Resistance-Type Sensor Exploration

In theoretical analysis, calculation formulas are usually used to directly reflect the sensitivity of gas-sensing materials to gases, but for Mo₂C, which has no band gap, it cannot be calculated and directly reflected by this method. The good adsorption characteristics of Mo₂C for all four gas molecules are indirectly known through the detailed analysis in the previous section, and this section intuitively reflects it from the theoretical recovery time.

The recovery time is the process of gas detachment from the sensor surface and its duration can be used to determine whether the material can be used as a basis for multiple gas detection over a long period of time. The recovery time (τ) can be calculated from the Van't Hoff Arrhenius formula [17].

$$\tau = A^{-1} e^{\left(\frac{E_a}{k_B T}\right)} \quad (3)$$

where A is the attempt frequency factor, whose magnitude is defined as 10^{12} (s⁻¹) [35], E_a (eV) is the potential barrier to be overcome for desorption, which here is equivalent to the opposite of the adsorption energy. k_B is the Boltzmann constant, and T is the operating temperature. Equation (3) shows that the larger the potential barrier to be overcome for desorption at the same temperature, the longer the desorption time; in other words, the smaller the adsorption energy and the more difficult it is to desorb. In addition, for the same material, the time for the gas to come off the surface of the gas-sensitive material can be shortened by increasing the working temperature. The desorption times of these four gases at 298 K, 398 K, 498 K and 598 K were calculated by Equation (3). For H₂S gas, when the temperature rises to 598 K, the desorption time is an ideal 13.9 s. For the other three gas molecules with smaller adsorption energy, the sensor recovery characteristics are not ideal when there is no external interference; it is necessary to increase the external conditions to enhance the recovery performance, and increase the life of the sensor. For example, when the sensor ends a service cycle, by adding high-power ultraviolet irradiation or high heat in an oxygen-rich environment, the desorption of the adsorbed gas is accelerated, increasing the repeatability of the sensor. In general, Mo₂C gas-sensitive materials are not suitable for resistive gas sensors. The next section will explore other applications in terms of low-power material properties.

3.4. Work Function (WF) Analysis

WF represents the minimum energy required for the transfer of electrons from the surface of the adsorbed substrate material to the vacuum [36]. This minimum energy determines the contact potential of the band arrangement between the gas molecules and the gas-sensitive material during the whole gas adsorption process [37]. This section will discuss the possibility of Mo₂C as a field-effect transistor sensor.

Figure 6 shows the WF of Mo₂C and the four adsorption systems, from which it can be seen that the trend of the work function changes differently for the adsorption of different gases [38]. In more detail, the WF of Mo₂C decreases to 4.56 eV after the adsorption of H₂S, and the WF of the system decreases to 4.71 after the adsorption of SO₂, indicating

that it is easier for electrons to escape from the Mo₂C surface to the vacuum layer after the adsorption of these two gases [39]. In contrast, the WF of the system increases to 4.96 eV and 5.04 eV after the adsorption of SOF₂ and SO₂F₂, respectively, which increases the difficulty of electron escape from the Mo₂C surface. The change in WF caused by gas adsorption shows that Mo₂C has the possibility of gas detection using Kelvin probe microscopy [40]. Since Mo₂C has two different WF trends for the four gases, this provides the possibility to explore Mo₂C as a field-effect transistor sensor for selective detection of SF₆ decomposition gases [41,42].

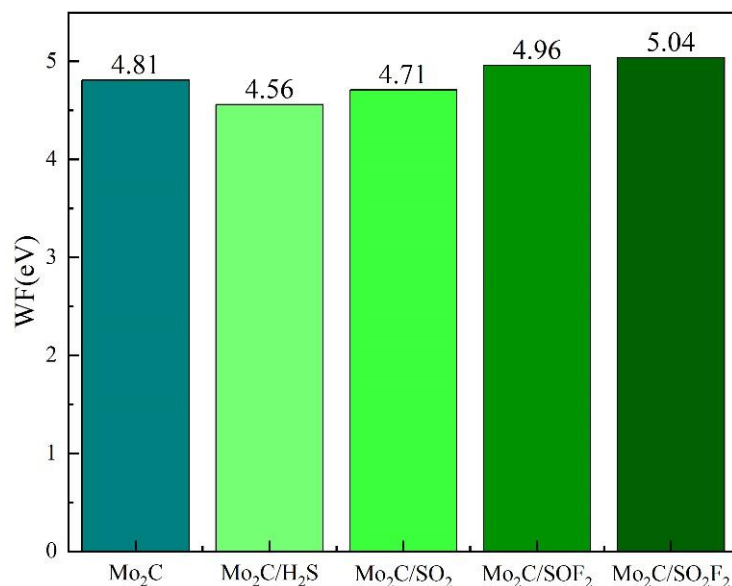


Figure 6. WF of adsorption systems.

4. Conclusions

First principles were employed to investigate the adsorption behavior of Mo₂C on H₂S, SO₂, SOF₂, and SO₂F₂ for sensing applications in the detection of SF₆ decomposition products. The whole research work is divided into three parts: firstly, the structure and properties of Mo₂C material are introduced; secondly, the adsorption behavior of four gas molecules on the Mo₂C surface is investigated; and finally, the sensing performance of Mo₂C for these four gases is comprehensively analyzed considering industrial applications. The results showed that H₂S, SO₂, SOF₂, and SO₂F₂ were successfully adsorbed on the Mo₂C surface with adsorption energies of −1.560 eV, −2.538 eV, −3.548 eV, and −4.944 eV, respectively, and their adsorption properties were determined by combining CDD and DOS analyses. The possibility of Mo₂C as a field-effect transistor sensor with good selectivity was found from WF calculations. Overall, the whole research work provides data to support the industrial application of Mo₂C as a microfluidic gas-sensitive sensor.

Author Contributions: L.L. carried out the calculations and wrote this manuscript, G.Z. conceived and designed the research, Z.W., J.Y. and S.T. helped analyze the data, Y.L. review and editing. All authors have read and agreed to the published version of the manuscript.

Funding: This research was funded by the Key Research and Development Pro gram of Hubei Province, China (No. 2020BAA02), Natural Science Foundation of Hubei Province (No. 2020CFB166).

Conflicts of Interest: The authors declare no conflict of interest.

References

1. Tang, J.; Rao, X.; Zeng, F.; Cai, W.; Cheng, L.; Zhang, C. Influence Mechanisms of Trace H₂O on the Generating Process of SF₆ Spark Discharge Decomposition Components. *Plasma Chem. Plasma Processing* **2017**, *37*, 325–340. [[CrossRef](#)]
2. Wu, Y.; Ding, D.; Wang, Y.; Zhou, C.; Lu, H.; Zhang, X. Defect recognition and condition assessment of epoxy insulators in gas insulated switchgear based on multi-information fusion. *Measurement* **2022**, *190*, 110701. [[CrossRef](#)]
3. Wang, Y.; Ding, D.; Zhang, Y.; Yuan, Z.; Tian, S.; Zhang, X. Research on infrared spectrum characteristics and detection technology of environmental-friendly insulating medium C5F10O. *Vib. Spectrosc.* **2022**, *118*, 103336. [[CrossRef](#)]
4. Zhang, X.; Liu, L.; Wang, J.; Wang, Z. Detection of SF₆ decomposition components by pristine and Cr-doped GaN based on the first-principles theory. *Comput. Theor. Chem.* **2021**, *1205*, 113431. [[CrossRef](#)]
5. Wang, J.; Zhang, X.; Liu, L.; Wang, Z. Adsorption of SF₆ Decomposition Products by the S Vacancy Structure and Edge Structure of SnS₂: A Density Functional Theory Study. *ACS Omega* **2021**, *6*, 28131–28139. [[CrossRef](#)] [[PubMed](#)]
6. Tang, J.; Liu, F.; Zhang, X.; Meng, Q.; Zhou, J. Partial discharge recognition through an analysis of SF₆ decomposition products part 1: Decomposition characteristics of SF₆ under four different partial discharges. *IEEE Trans. Dielectr. Electr. Insul.* **2012**, *19*, 29–36. [[CrossRef](#)]
7. Tang, J.; Liu, F.; Meng, Q.; Zhang, X.; Tao, J. Partial discharge recognition through an analysis of SF₆ decomposition products part 2: Feature extraction and decision tree-based pattern recognition. *IEEE Trans. Dielectr. Electr. Insul.* **2012**, *19*, 37–44. [[CrossRef](#)]
8. Li, Y.; Zhang, X.; Chen, D.; Xiao, S.; Tang, J. Adsorption behavior of COF₂ and CF₄ gas on the MoS₂ monolayer doped with Ni: A first-principles study. *Appl. Surf. Sci.* **2018**, *443*, 274–279. [[CrossRef](#)]
9. Ding, K.; Lin, Y.; Huang, M. The enhancement of NO detection by doping strategies on monolayer MoS₂. *Vac. Technol. Appl. Ion Phys. Int. J. Abstr. Serv. Vac. Sci. Technol.* **2016**, *130*, 146–153.
10. Wang, J.; Zhang, X.; Liu, L.; Wang, Z. Dissolved gas analysis in transformer oil using Ni-Doped GaN monolayer: A DFT study. *Superlattices Microstruct.* **2021**, *159*, 107055. [[CrossRef](#)]
11. Kadioglu, Y.; Ersan, F.; Kecik, D.; Aktürk, O.; Aktürk, E.; Ciraci, S. Chemical and substitutional doping, and anti-site and vacancy formation in monolayer AlN and GaN. *Phys. Chem. Chem. Phys.* **2018**, *20*, 16077–16091. [[CrossRef](#)] [[PubMed](#)]
12. Feng, C.; Qin, H.; Yang, D.; Zhang, G. First-Principles Investigation of the Adsorption Behaviors of CH₂O on BN, AlN, GaN, InN, BP, and P Monolayers. *Materials* **2019**, *12*, 676. [[CrossRef](#)] [[PubMed](#)]
13. Meng, R.; Lu, X.; Ingebrandt, S.; Chen, X. Adsorption of Gas Molecules on Graphene-Like ZnO Nanosheets: The Roles of Gas Concentration, Layer Number, and Heterolayer. *Adv. Mater. Interfaces* **2017**, *4*, 1700647. [[CrossRef](#)]
14. Gönüllü, Y.; Haidry, A.A.; Saruhan-Brings, B.J.S. Nanotubular Cr-doped TiO₂ for use as high-temperature NO₂-selective gas sensor. *Sens. Actuators B Chem.* **2015**, *217*, 78–87. [[CrossRef](#)]
15. Cho, S.-Y.; Kim, J.Y.; Kwon, O.; Kim, J.; Jung, H.-T. Molybdenum carbide chemical sensors with ultrahigh signal-to-noise ratios and ambient stability. *J. Mater. Chem. A* **2018**, *6*, 23408–23416. [[CrossRef](#)]
16. Wang, T.; Tian, X.; Yang, Y.; Li, Y.-W.; Wang, J.; Beller, M.; Jiao, H. Coverage dependent adsorption and co-adsorption of CO and H₂ on the CdI₂-antitype metallic Mo₂C(001) surface. *Phys. Chem. Chem. Phys.* **2014**, *17*, 1907–1917. [[CrossRef](#)]
17. Hassan, A.; Ilyas, S.Z.; Ahmed, S.; Niaz, F.; Jalil, A.; Khan, Q. Ab-initio study of molybdenum carbide (Mo₂C) as an adsorption-based filter. *Phys. Lett. A* **2021**, *392*, 127119. [[CrossRef](#)]
18. Zhang, D.; Tong, J.; Xia, B. Humidity-sensing properties of chemically reduced graphene oxide/polymer nanocomposite film sensor based on layer-by-layer nano self-assembly. *Sens. Actuators B Chem.* **2014**, *197*, 66–72. [[CrossRef](#)]
19. Zhang, D.; Sun, Y.E.; Li, P.; Zhang, Y. Facile fabrication of MoS₂-modified SnO₂ hybrid nanocomposite for ultrasensitive humidity sensing. *ACS Appl. Mater. Interfaces* **2016**, *8*, 14142–14149. [[CrossRef](#)]
20. Zhang, X.; Yu, L.; Wu, X.; Hu, W. Experimental Sensing and Density Functional Theory Study of H₂S and SOF₂ Adsorption on Au-Modified Graphene. *Adv. Sci.* **2015**, *2*, 1500101. [[CrossRef](#)]
21. Yang, Q.-L.; Ban, Y.-L.; Lian, J.-W.; Yu, Z.-F.; Wu, B. SIW Butler Matrix with Modified Hybrid Coupler for Slot Antenna Array. *IEEE Access* **2016**, *4*, 9561–9569. [[CrossRef](#)]
22. Cui, H.; Zheng, K.; Tao, L.; Yu, J.; Zhu, X.; Li, X.; Chen, X. Monolayer Tellurene-Based Gas Sensor to Detect SF₆ Decompositions: A First-Principles Study. *IEEE Electron Device Lett.* **2019**, *40*, 1522–1525. [[CrossRef](#)]
23. Wang, Y.; Zhang, D.; Han, J.; Yang, Y.; Guo, Y.; Bai, Z.; Cheng, J.; Chu, P.K.; Pang, H.; Luo, Y. Porous Mo₂C-Mo₃N₂ heterostructure/rGO with synergistic functions as polysulfides regulator for high-performance lithium sulfur batteries. *Chem. Eng. J.* **2021**, *433*, 133629. [[CrossRef](#)]
24. Zhang, D.; Yu, S.; Wang, X.; Huang, J.; Pan, W.; Zhang, J.; Meteku, B.E.; Zeng, J. UV illumination-enhanced ultrasensitive ammonia gas sensor based on (001)TiO₂/MXene heterostructure for food spoilage detection. *J. Hazard. Mater.* **2022**, *423*, 127160. [[CrossRef](#)]
25. Zhang, Y.-H.; Han, L.-F.; Xiao, Y.-H.; Jia, D.-Z.; Guo, Z.-H.; Li, F. Understanding dopant and defect effect on H₂S sensing performances of graphene: A first-principles study. *Comput. Mater. Sci.* **2013**, *69*, 222–228. [[CrossRef](#)]
26. Liu, Y.; Zhou, Q.; Mi, H.; Wang, J.; Zeng, W. Gas-sensing mechanism of Cr doped SnP₃ monolayer to SF₆ partial discharge decomposition components. *Appl. Surf. Sci.* **2021**, *546*, 149084. [[CrossRef](#)]
27. Zhang, X.; Wang, J.; Chen, D.; Liu, L. The adsorption performance of harmful gas on Cu doped WS₂: A first-principle study. *Mater. Today Commun.* **2021**, *28*, 102488. [[CrossRef](#)]
28. Sun, X.; Yang, Q.; Meng, R.; Tan, C.; Liang, Q.; Jiang, J.; Ye, H.; Chen, X. Adsorption of gas molecules on graphene-like InN monolayer: A first-principle study. *Appl. Surf. Sci.* **2017**, *404*, 291–299. [[CrossRef](#)]

29. Ma, S.; Li, D.; Rao, X.; Xia, X.; Su, Y.; Lu, Y. Pd-doped h-BN monolayer: A promising gas scavenger for SF₆ insulation devices. *Adsorption* **2020**, *26*, 619–626. [[CrossRef](#)]
30. Chen, D.; Zhang, X.; Tang, J.; Cui, H.; Li, Y. Noble metal (Pt or Au)-doped monolayer MoS₂ as a promising adsorbent and gas-sensing material to SO₂, SOF₂ and SO₂F₂: A DFT study. *Appl. Phys. A* **2018**, *124*, 194. [[CrossRef](#)]
31. Gui, Y.; Shi, J.; Yang, P.; Li, T.; Tang, C.; Xu, L. Platinum modified MoS₂ monolayer for adsorption and gas sensing of SF₆ decomposition products: A DFT study. *High Volt.* **2020**, *5*, 454–462. [[CrossRef](#)]
32. Cui, H.; Chen, D.; Zhang, Y.; Zhang, X. Dissolved gas analysis in transformer oil using Pd catalyst decorated MoSe₂ monolayer: A first-principles theory. *Sustain. Mater. Technol.* **2019**, *20*, e00094. [[CrossRef](#)]
33. Liu, X.; Ni, Y.X.; Wang, H.Y.; Wang, H. Tuning structural, electronic, and magnetic properties of black-AsP monolayer by adatom adsorptions: A first principles study. *Chin. J. Chem. Phys.* **2020**, *33*, 311–318. [[CrossRef](#)]
34. Cui, H.; Zhang, X.; Chen, D.; Tang, J. Pt & Pd decorated CNT as a workable media for SOF₂ sensing: A DFT study. *Appl. Surf. Sci.* **2018**, *471*, 335–341. [[CrossRef](#)]
35. Liu, Z.; Gui, Y.; Xu, L.; Chen, X. Adsorption and sensing performances of transition metal (Ag, Pd, Pt, Rh, and Ru) modified WSe₂ monolayer upon SF₆ decomposition gases (SOF₂ and SO₂F₂). *Appl. Surf. Sci.* **2021**, *581*, 152365. [[CrossRef](#)]
36. Zhu, H.; Cui, H.; He, D.; Cui, Z.; Wang, X. Rh-doped MoTe₂ Monolayer as a Promising Candidate for Sensing and Scavenging SF₆ Decomposed Species: A DFT Study. *Nanoscale Res. Lett.* **2020**, *15*, 129. [[CrossRef](#)]
37. Sun, H.; Tao, L.-Q.; Li, T.; Gao, X.; Wang, G.; Peng, Z.; Zhu, C.; Zou, S.; Gui, Y.; Xia, S.-Y.; et al. Sensing Characteristics of Toxic C₄F₇N Decomposition Products on Metallic- Nanoparticle Co-Doped BN Monolayer: A First Principles Study. *IEEE Sens. J.* **2021**, *21*, 13082–13089. [[CrossRef](#)]
38. Guo, H.; Zhang, F.; Qiu, J.; Wu, L.; Zhu, B.; Chen, X.; Yu, J. PbSnS₂-Based Gas Sensor to Detect SF₆ Decompositions: DFT and NEGF Calculations. *IEEE Trans. Electron Devices* **2021**, *68*, 5322–5325. [[CrossRef](#)]
39. Cui, H.; Zhang, G.; Zhang, X.; Tang, J. Rh-doped MoSe₂ as a toxic gas scavenger: A first-principles study. *Nanoscale Adv.* **2018**, *1*, 772–780. [[CrossRef](#)]
40. Liu, W.; Qiu, X.; Song, Y.; Zhang, X.; Tian, S.; Liu, L. Adsorption behaviour of CF₄ and COF₂ gas on the GaN monolayer doped with Pt catalytic: A first-principles study. *Surf. Sci.* **2022**, *719*, 122032. [[CrossRef](#)]
41. Zhang, G.Z.; Wang, Z.T.; Zhang, X.X. Theoretical screening into Ru-doped MoS₂ monolayer as a promising gas sensor upon SO₂ and SOF₂ in SF₆ insulation devices. *Mol. Phys.* **2022**, *120*, 8. [[CrossRef](#)]
42. Kou, L.; Tang, C.; Zhang, Y.; Heine, T.; Chen, C.; Frauenheim, T. Tuning Magnetism and Electronic Phase Transitions by Strain and Electric Field in Zigzag MoS₂ Nanoribbons. *J. Phys. Chem. Lett.* **2012**, *3*, 2934–2941. [[CrossRef](#)] [[PubMed](#)]